IEEE Access
Multidisciplinary ⋮ Rapid Review ⋮ Open Access Journal

Received 6 June 2022, accepted 27 June 2022, date of publication 28 July 2022, date of current version 4 August 2022.

Digital Object Identifier 10.1109/ACCESS.2022.3194708

RESEARCH ARTICLE

60-GHz Wideband L-Probe Circular Slotted E-Shaped Patch Antenna Array

TAEHWAN JANG[1], (Member, IEEE), AND CHUL SOON PARK[2]
[1]School of Electronic Engineering, Hanyang University, Ansan 15588, Republic of Korea
[2]School of Electrical Engineering, Korea Advanced Institute of Science and Technology (KAIST), Daejeon 305-730, South Korea

Corresponding author: Taehwan Jang (hundredwin@hanyang.ac.kr)

This work was supported in part by the National Research Foundation of Korea (NRF) Grant by the Korea Government through the Ministry of Science, ICT and Future Planning (MSIP), under Grant 2021R1A2C2095377 and Grant 2022R1F1A1072517; and in part by the Institute of Information and Communications Technology Planning and Evaluation (IITP) Grant through the Korea Government (MSIT) (Development of High Resolution Vector Network Analyzer HW Platform Supporting Sub-THz Frequency Band, 33.3%) under Grant 2022-0-00868.

ABSTRACT In this study, a 60-GHz wideband L-probe circular slotted E-shaped patch antenna array was presented. The novelty of this study can be summarized as follows: 1) An E-shaped patch was added to the L-probe to further expand the bandwidth of the existing L-probe patch. 2) The E-shaped slot was modified to a circular slot to improve the overall performance, including the radiation pattern, S_{11}, and cross-polarization of the original E-shaped patch antenna element. When compared to the original L-probe patch, the bandwidth was improved from 9.4% to 24.8% for the proposed antenna element. Furthermore, when compared with the triangular-shaped and rectangular-shaped slots, the cross-polarization level is improved by 3.5 dB and 2.5 dB, respectively. The proposed antenna was designed as a 2×2 array structure, and the size of the antenna array corresponded to 6.4 mm $\times$ 6.4 mm $\times$ 0.375 mm. The measured results of the proposed antenna array revealed 11.42 dBi peak gain, 25.8% fractional 3-dB gain bandwidth, and 44.7% -8 dB S_{11} bandwidth.

INDEX TERMS Wideband, E-shaped patch, L-probe patch, cross polarization, antenna array, circular slot, 60-GHz.

I. INTRODUCTION

In 2001, the US Federal Communications Commission allotted a continuous section of the spectrum (57–64 GHz) for wireless communication [1]. Using this frequency band, it is possible to transmit and receive up to tens of Gbps of data [2]–[6] for uncompressed video, voice, and data content. To cover this 60-GHz industrial, scientific, and medical (ISM) band, the antenna should cover the entire ISM band, ranging from 57 to 64 GHz. To cover the 57-64GHz bandwidth, a wideband antenna should be proposed with good radiation performance. For mobile applications using this frequency band, patch antennas are preferred because of their low profile and robust characteristics.

However, the bandwidth of the original patch antenna is as small as <10%, making it difficult to cover 60-GHz unlicensed bands. Therefore, the following techniques were applied to the patch antenna to expand the bandwidth further. Based on previous studies, the bandwidths of patch antennas can be improved by using a patch with U-slot [7]–[10], E-shaped patch antenna [11]–[15], L-probe patch antenna [16]–[20], adding parasitic patches [21]–[24], and horn antenna structure [25].

In case of 60-GHz frequency band, many types of antenna is presented [9], [25]–[30]. For the 60-GHz U-shaped patch antenna [9], it was reported that the impedance bandwidth can be improved by up to 15% fractional bandwidth by adding a resonance frequency point generated by a U-shaped slot.

In the case of the 60-GHz E-shaped patch antenna, the impedance bandwidth can be expanded by up to 21.7%. Furthermore, the improvement in bandwidth is due to the additional resonance frequency of the rectangular slots at the E-shaped patch. However, there is a disadvantage that the radiation characteristic is deteriorated at the resonance point generated by the rectangular slot.

The associate editor coordinating the review of this manuscript and approving it for publication was Tutku Karacolak.

Moreover, the impedance bandwidth can be expanded by applying the L-probe technique [17].

In [22], the addition of a parasitic strip with an E-shaped patch antenna extended the impedance bandwidth but did not increase the gain bandwidth because the current through the parasitic strip flowed in the opposite direction of the patch antenna.

For horn structure in the 60-GHz band [25], the impedance bandwidth can be improved, but additional processing costs are incurred because of the complex antenna structure.

In this study, a novel antenna element is proposed by combining the advantages of the L-probe antenna and E-shaped patch with a circular slot structure. An ultra-wideband antenna element and array are designed with several resonance points due to E-shaped patches and L-probe structures. The effect of widening the bandwidth of each structure is analyzed in detail. Moreover, to improve the overall performance, including the radiation pattern, S_{11}, and cross-polarization of the conventional E-shaped antenna element, the slots are modified to a circular shape, and these effects are analyzed in detail in this study. In Section II, an analysis of the proposed structure is presented. In Section III, the simulated and measured performances of the proposed antenna array are presented, and the paper is concluded in Section IV.

II. ANTENNA DESIGN

A. ANTENNA GEOMETRY

Fig. 1 shows the geometry of the 60-GHz L-probe circular slotted E-shaped patch antenna element and array. In this study, the L-probe feeding topology was applied to a wideband E-shaped patch antenna with an additional resonance point. This is explained in section II-B. The shape of the slot is modified to a circular geometry to further improve the overall characteristic (impedance bandwidth, 3-dB gain bandwidth, radiation pattern, and cross-polarization) of the E-shaped patch antenna, which will be described in Section II-C. The ground-signal-ground (G-S-G) pad is placed at the antenna feeding to ensure contact with the G-S-G probe for antenna measurement. In this study, a 2×2 antenna array is designed to realize a high gain to compensate for the path loss of the 60-GHz band, and a conventional parallel feeding network using quarter-wave transformers is applied. The antenna was designed using the full-wave electro-magnetic solver Ansoft HFSS and was optimized using the optimetrics function of Ansoft HFSS.

A GFPL-970LF substrate, which is built in a 6-layer PCB stack, comprises five 60-μm thick substrate. The thickness of the copper layer is 15 μm. The dielectric permittivity (ε_r) of the GFPL-970LF substrate is 3.27, and the loss tangent is 0.009. The overall thickness of the proposed antenna is designed as 0.375 mm for a short bond-wire interconnection with 300-um thick RFIC. The proposed antenna is simulated and optimized via a 3-D full wave simulator.

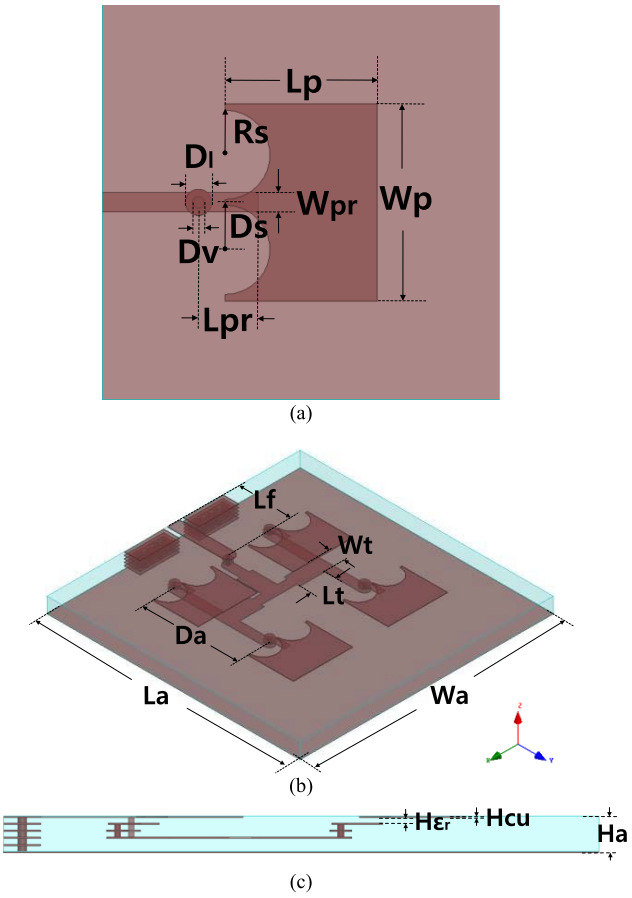

FIGURE 1. Geometry of the 60-GHz L-probe, circular slotted E-shaped patch antenna element and array. (a) antenna element and (b) antenna array (c) the sectional view of the array antenna. The parameter dimensions in millimeters are Wp=1.5, Lp=1.15, Rs=0.34, Ds=0.36, Dl=0.2, Dv=0.09, Lpr=0.45, Wpr=0.15, Wt=0.4, Lt=0.63, Lf=1.375, Da=2.4, La=6.4, Wa=6.4, $H\varepsilon_r$=0.06, Hcu=0.015 and Ha=0.375.

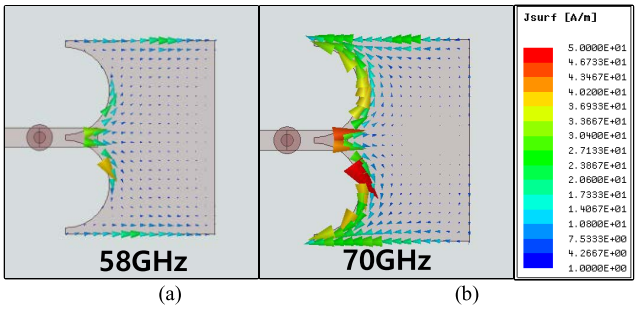

FIGURE 2. Current distribution of the proposed antenna element at (a) 58 GHz and (b)70 GHz.

B. BANDWIDTH EXPANSION WITH L-PROBED E-SHAPED PATCH STRUCTURE

It was reported that the L-probe feed [16]–[20] structure and E-shaped patch antenna [11]–[15] expand the bandwidth of the antenna. In this study, a wideband E-shaped patch antenna is fed by an L-probe to further improve the bandwidth of the antenna by creating additional resonance points.

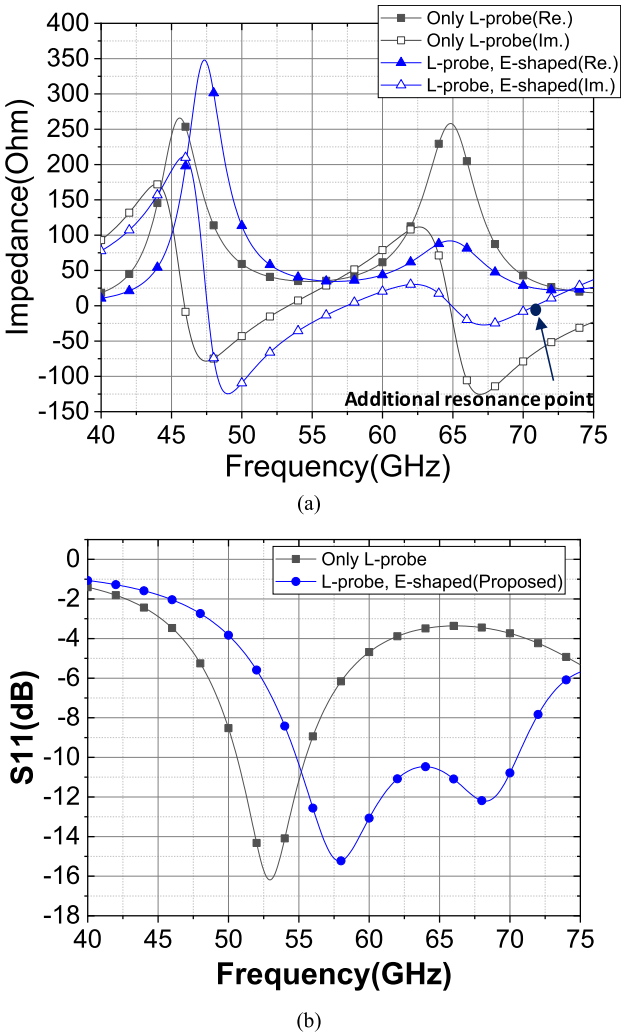

FIGURE 3. Comparison between L-probe patch and proposed L-probe E-shaped patch antenna element. (a) Impedance and (b) S11.

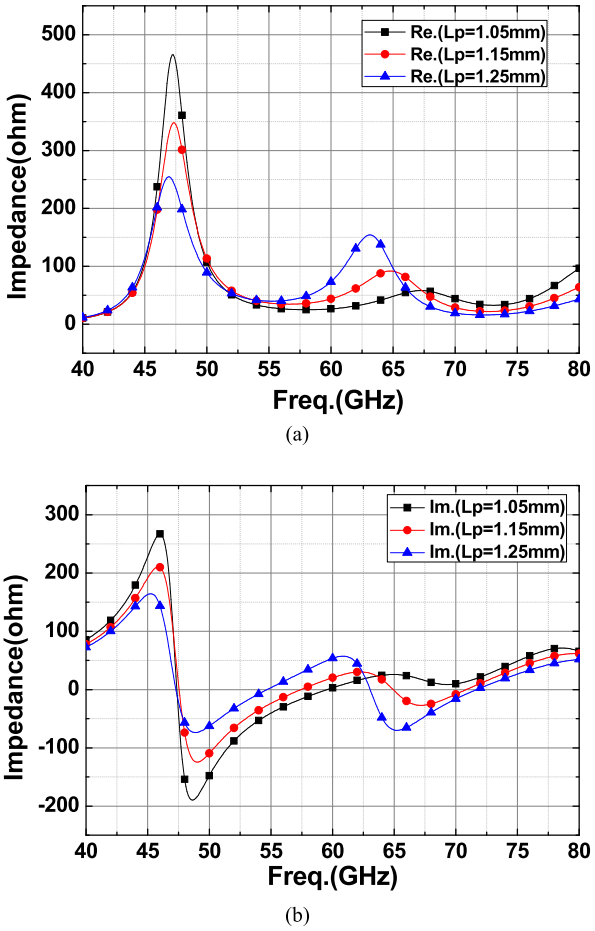

FIGURE 4. Simulated (a)real and (b)imaginary impedance of the antenna element obtained by sweeping Lp.

Fig. 2 shows the current distribution of the proposed antenna element at 58 GHz and 70 GHz. It is clearly observed that the rectangular patch exhibits a half-wave resonance at 58 GHz, and resonance does not occur in the circular patch. Moreover, at 70-GHz, half-wave resonance occurs in the circular slot, and the patch is out of resonance. It is expected that the imaginary input impedance becomes zero by causing resonance at these two resonance frequencies. Fig. 3 shows a comparison between the L-probe patch and proposed L-probe E-shaped patch antenna element. In case of the only L-probe case, S_{11} forms a narrow bandwidth of 4.9 GHz(=9.4%) from 50.6 GHz to 55.5 GHz. However, in the case of the proposed L-probe E-shaped patch, it can be observed that the bandwidth is widened to 15.6 GHz(=24.8%) ranging from 54.9 GHz to 70.5 GHz by the resonant frequency added by the circular slot. This is the fundamental difference between the proposed antenna and L-probe antenna.

Fig. 4 shows the simulated real and imaginary impedances of the antenna element obtained by sweeping L_p. The other parameters of the antenna, with the exception of L_p, were determined using the final dimensions shown in Fig. 1. There are four resonance points at 47.5 GHz, 57.5 GHz, 65 GHz, and 71 GHz. The first resonance point at 47.5 GHz($=f_{1,c}$) originated from the L-probe feed. The second resonance at 57.5 GHz($=f_{2,c}$) is the fundamental half-wave resonance of the rectangular patch, and the third resonance at 65 GHz($=f_{3,c}$) is a high-order resonance point from the rectangular patch. The fourth resonance point at 71 GHz($=f_{4,c}$) originated from the circular slot. The $f_{2,c}$ and $f_{3,c}$ frequencies formed by rectangular patches move dominantly by sweeping L_p, whereas $f_{1,c}$ and $f_{4,c}$ hardly change.

Fig. 5 shows the simulated real and imaginary impedances of the antenna element obtained by sweeping R. The f_4 frequency formed by the circular slot moves dominantly by sweeping R, whereas $f_{1,c}$ and $f_{3,c}$ hardly change. When R_s changes from 0.24 mm to 0.34 mm, $f_{2,c}$ is upshifted from 55 GHz to 57.5 GHz. This is due to the fact that four times the radius of the circular slot($=4R_s$) has a value similar to W_p, resulting in a reduction in the effective length of the patch as shown in Fig. 1(a). When R_s changes from 0.24 mm to 0.34 mm, $f_{1,c}$ is also upshifted from 46 GHz to 47.5 GHz.

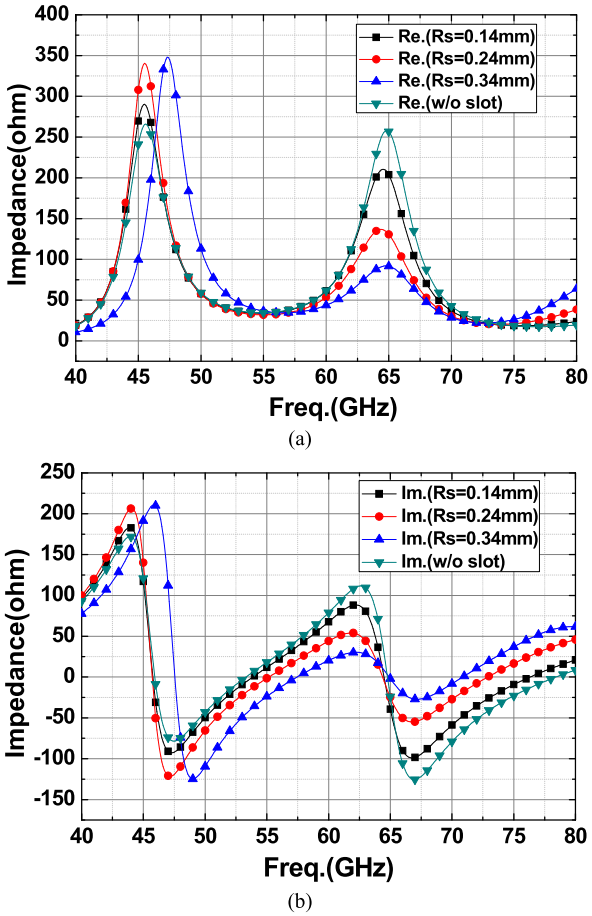

FIGURE 5. Simulated (a)real and (b)imaginary impedance of the antenna element obtained by sweeping Rs.

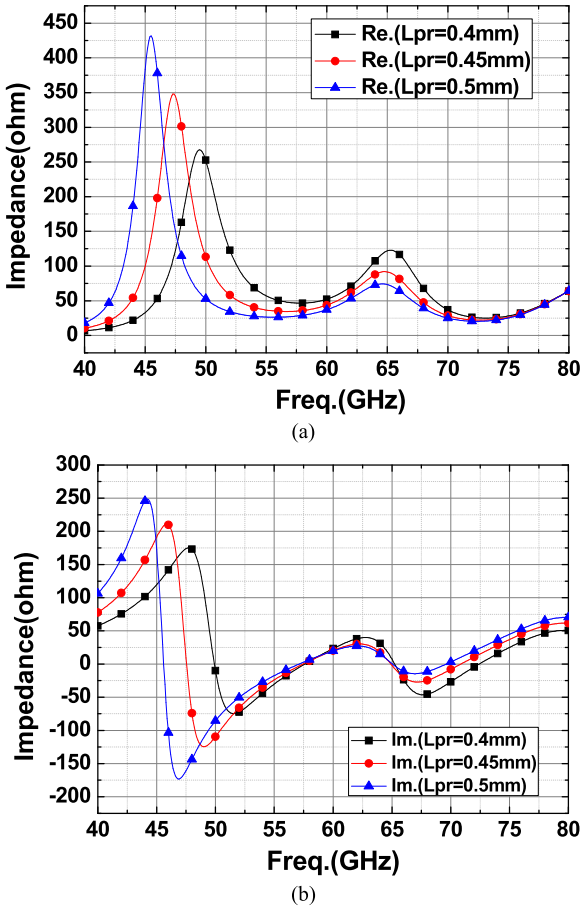

FIGURE 6. Simulated (a)real and (b)imaginary impedance of the antenna element obtained by sweeping Lpr.

This phenomenon is also due to the changes in the effective feeding point because the size of the rectangular patch on the L-probe side decreases owing to the larger slot size.

Fig. 6 shows the simulated real and imaginary impedances of the antenna element obtained by sweeping L_{pr}. In this case, only $f_{1,c}$ move dominantly as L_{pr} changes. The parametric simulation in Fig. 3, 4, and 5 shows the parameter on which each resonance point ($f_{1,c}$, $f_{2,c}$, $f_{3,c}$, and $f_{4,c}$,) is dependent.

C. FURTHER PERFORMANCE IMPROVEMENT USING E-SHAPED PATCH ANTENNA WITH CIRCULAR SHAPED SLOT

Fig. 7 shows the geometry and simulated current distribution at 70 GHz for an E-shaped patch antenna element with triangular, rectangular, and circular slots. The dimensions of the triangular, rectangular, and circular slots were optimized to maximize the −10-dB S_{11} bandwidth. If a circular slot is used, then the S_{11} and gain bandwidth can be widened, and the cross-polarization level is improved when compared to that of the rectangular or triangular case. This can be explained as follows.

Assuming that the frequencies ($f_{4,c}$, $f_{4,r}$, and $f_{4,t}$) are the same, the lengths of each slot can be the same, and the following equation is satisfied.

$$\pi R_S = W_{re} + 2L_{re} = 2D_{tr} \tag{1}$$

In this case, the area of the circular slot is always $\frac{4}{\pi}$ times that in the rectangular and triangular cases.

$$\frac{\pi R_s^2}{2} \geq \frac{4}{\pi} W_{re} L_{re} \tag{2}$$

$$\frac{\pi R_s^2}{2} \geq \frac{4}{\pi} \frac{D_{tr}^2}{2} \sin\theta \tag{3}$$

Frequencies $f_{4,c}$, and $f_{4,r}$, correspond to the length of each slot, and it is assumed that the lengths of the circular and rectangular slots are equal.

$$\pi R_s = W_{re} + 2L_{re} \tag{4}$$

If the arithmetic–geometric mean (AGM) method is applied to (4), the following inequality is satisfied:

$$(\pi R_s)^2 = (W_{re} + 2L_{re})^2 \geq 8 W_{re} L_{re} \tag{5}$$

Eq. (5) is also modified as follows:

$$\frac{\pi R_s^2}{2} \geq \frac{4}{\pi} W_{re} L_{re} > W_{re} L_{re} \tag{6}$$

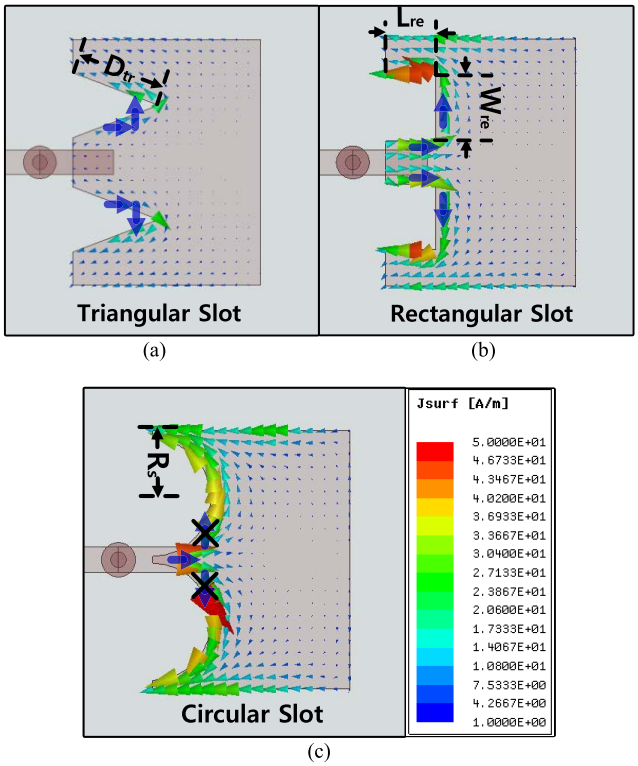

FIGURE 7. Geometry and simulated current distribution for E-shaped patch antenna element with (a)triangular slot, (b) rectangular slot and (c) circular slot. The current distribution is simulated at 70GHz. The parameter dimensions in millimeters are Dtr=0.53, Lre=0.3 and Wre=0.4.

This implies that the area of the circular slot is at least $\frac{4}{\pi}$ times larger than that of the rectangular slot. Therefore, the space between the two slots remained as low as the original area, with the exception for the slots, thereby improving the performance of the proposed antenna element.

Similarly assuming that frequencies $f_{4,c}$ and $f_{4,t}$ are the same, the following equation is satisfied:

$$\pi R_s = 2D_{tr} \tag{7}$$

Eq. (7) is also re-expressed as follows:

$$\frac{\pi R_s^2}{2} = \frac{2}{\pi}D_{tr}^2 \geq \left(\frac{4}{\pi}\right)\left(\frac{1}{2}D_{tr}^2\right) > \frac{1}{2}D_{tr}^2 \sin\theta \tag{8}$$

This implies that the area of the circular slot is at least $\frac{4}{\pi}$ times larger than that of the triangular slot and also exhibits a performance improvement when compared to that of the triangular slot. From (2) and (3), the area between the two slots remains smaller in the circular slot case than in the rectangular and triangular cases. Therefore, among the currents flowing between slots, x- or –x- polarized current components flowing in opposite directions neutralize each other, which mostly occurs in the case of circular slots. This phenomenon explains as to why the cross-polarization can be reduced for the circular slot case as opposed to that for the rectangular or triangular slot.

Additionally, the current component flowing in the y-direction (which is opposite to the polarization of the main patch) becomes close in the circular slot case, and the array factor of the current components flowing in the y-direction is the smallest. This contributes to less distortion of the radiation pattern.

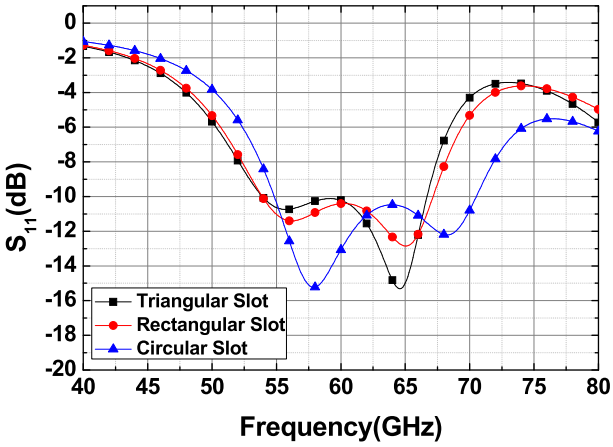

FIGURE 8. Simulated S11 for E-shaped patch antenna element with (a)triangular slot, (b) rectangular slot and (c) circular slot.

Moreover, in the case of triangular and square slots, the impedance near $f_{4,t}$ or $f_{4,r}$ frequency formed by the slot changes rapidly because each vertex exhibits a discontinuity in the slot's geometry. However, in the case of the circular patch, the impedance changes slowly around the $f_{4,c}$ frequency. Hence, the S_{11} bandwidth is wider than when the triangular or rectangular slot is applied to the E-shaped patch antenna element.

Fig. 8 shows the simulated S_{11} for an E-shaped patch antenna element with triangular, rectangular, and circular slots. For the triangular case, the −10-dB S_{11} bandwidth is 12.7 GHz (=21.0% fractional BW), ranging from 54 GHz to 66.7 GHz. In case of the rectangular slot, −10-dB S_{11} bandwidth is 13.2 GHz (=21.8% fractional BW) ranging from 53.9 GHz to 67.2 GHz. Finally, the S_{11} bandwidth is 15.7 GHz(=25.1% fractional BW) ranging from 54.8 GHz to 70.5 GHz for the circular slot case.

Fig. 9 shows the simulated radiation pattern for an E-shaped patch antenna element with triangular, rectangular, and circular slots at 70 GHz. For the triangular slot case, the radiation pattern is evidently distorted with the null point in a specific direction(at $\theta = 30°$, $\phi = 90°$). In the case of a rectangular slot, the null point disappears from the radiation pattern although the beam is broadly radiated into the H-plane. When a circular slot is used, the beam is evenly radiated without distortion of the radiation pattern.

Fig. 10 shows the simulated directivity and realized gain for an E-shaped patch antenna element with triangular, rectangular, and circular slots. The radiation pattern around the resonant frequency of the slot (f4) is improved by using the circular slot, and thus the direct slot and realized gain bandwidth are the widest for the circular slot. When compared with the triangular and rectangular slots, 5-GHz and 3-GHz of the 3-dB realized gain bandwidth are improved, respectively.

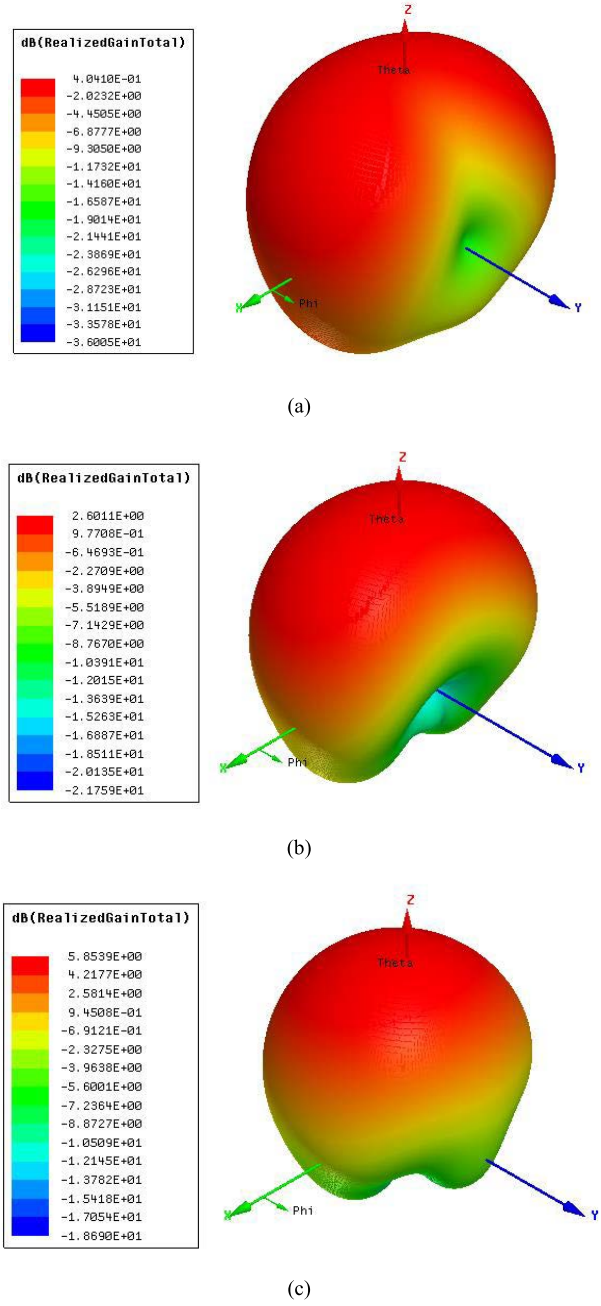

FIGURE 9. Simulated radiation pattern for E-shaped patch antenna element with (a)triangular slot, (b) rectangular slot and (c) circular slot. The radiation pattern is simulated at 70GHz.

Fig. 11 shows the simulated co-polarized and cross-polarized H-plane radiation patterns for an E-shaped patch antenna element with triangular, rectangular, and circular slots at 60 GHz. In the case of the E-shaped patch antenna, the addition of a rectangular slot to widen the bandwidth cuts the magnetic current, thereby exacerbating cross-polarization. The slot was revised to a circular shape to improve the cross-polarization when compared with that of the original E-shaped patch antenna with a rectangular slot.

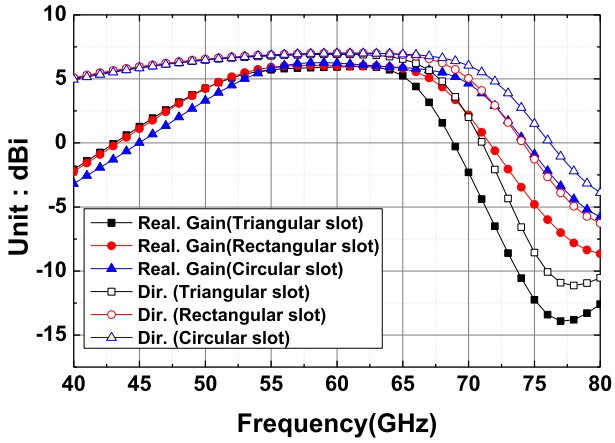

FIGURE 10. Simulated directivity and realized gain for E-shaped patch antenna element with (a)triangular slot, (b) rectangular slot and (c) circular slot.

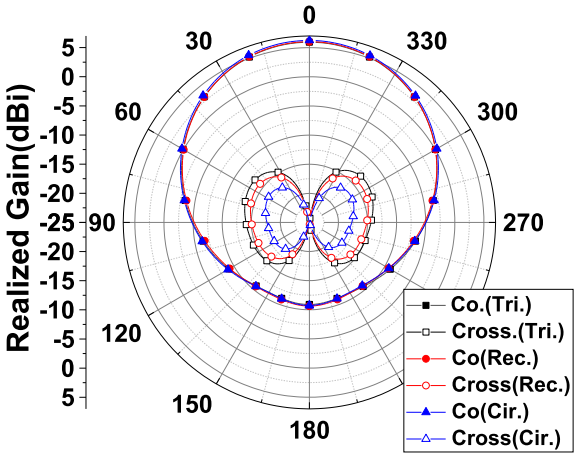

FIGURE 11. Simulated co-polarized and cross-polarized H-plane radiation pattern for E-shaped patch antenna element with triangular slot, rectangular slot and circular slot. The radiation pattern is simulated at 60GHz.

The co-polarization radiation pattern is constant irrespective of the shape of the slot, whereas the lowest cross-polarization is observed when circular-shaped slots are applied. When compared with the case of the triangular-shaped and rectangular-shaped slots, 3.5 dB and 2.5 dB of the cross-polarization level exhibit improvement, respectively.

III. ANTENNA MEASUREMENT

Fig. 12 shows the fabricated 60-GHz L-probed E-shaped antenna array with circular slots. The size of the antenna is 6.4 mm $\times$ 6.4 mm $\times$ 0.375 mm, corresponding to $1.28\,\lambda_0 \times 1.28\lambda_0 \times 0.075\lambda_0$. The reflection coefficient of the antenna array is measured using a vector network analyzer, and the radiation patterns of the fabricated antenna array are measured via a far-field millimeter-wave antenna measurement setup as shown in Fig. 13, which works in the V band. The radiation pattern was measured using a conventional gain comparison method with two identical

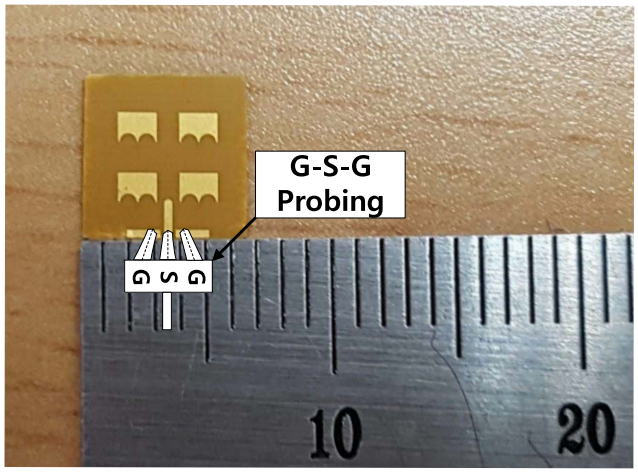

FIGURE 12. Fabricated antenna array.

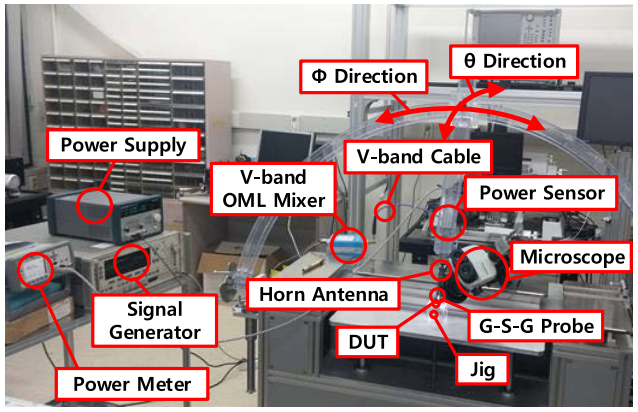

FIGURE 13. Measurement setup for radiation pattern.

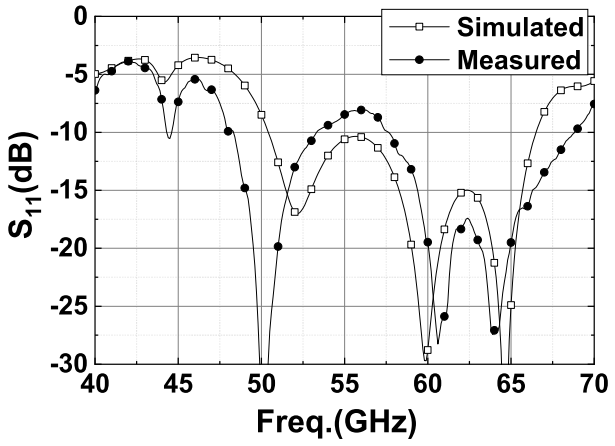

FIGURE 14. Simulated and measured S_{11} for the proposed antenna array.

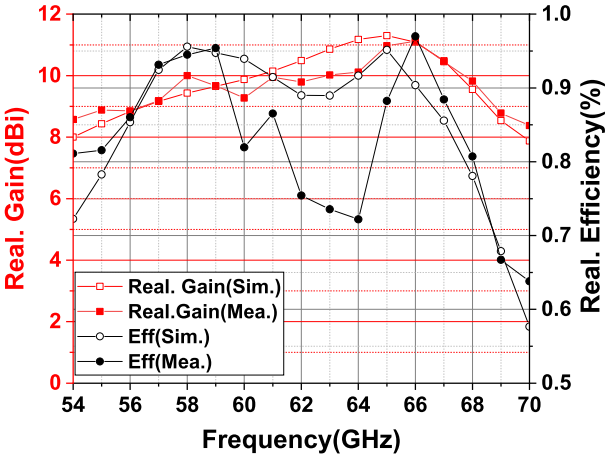

FIGURE 15. The simulated and measured realized gain and realized efficiency for the proposed antenna array.

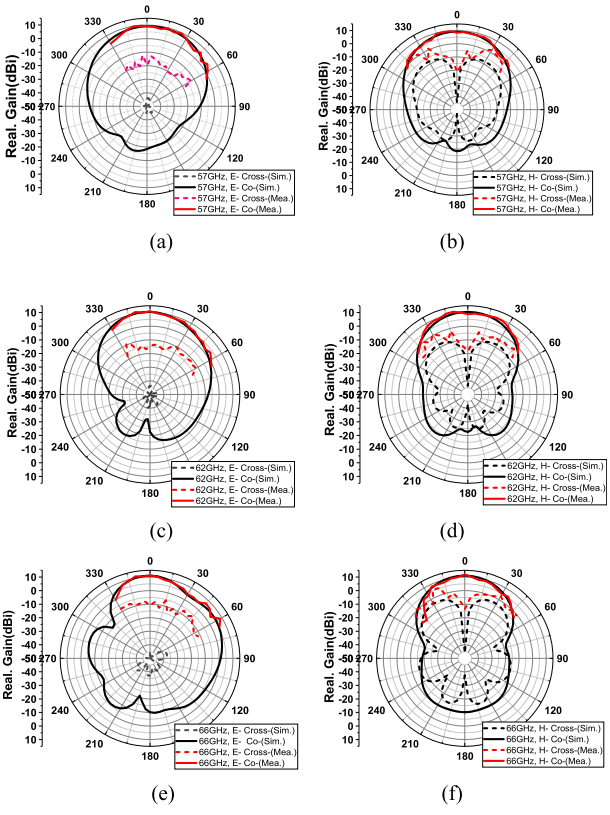

FIGURE 16. Simulated and measured E-plane and H-plane radiation patterns for 57 GHz, 62 GHz and 66 GHz for the proposed antenna array. (a) 57-GHz E-plane, (b) 57-GHz H-plane, (c) 62-GHz E-plane, (d) 62-GHz H-plane, (e) 66-GHz E-plane, and (f) 66-GHz H-plane.

standard pyramidal horn antennas. A 12.5–18.75 GHz signal was generated from the signal generator, and V-band OML mixer up-converted this signal to the 50–75 GHz band. This signal finally reaches the G-S-G probe flowing through the V-band cable. When the probe contact to the antenna under test, the antenna radiates the electromagnetic field and the reference horn antenna sense the received power. The horn antenna is connected with power sensor and can move in both the θ and ϕ directions, so that the radiation pattern can be measured. In the case of E-plane, it is impossible to measure the radiation pattern in the region where θ is smaller than $-30°$ due to the space of the probing system. In addition, when θ is greater than 60°, the signal reflected from the

TABLE 1. Comparison with previously reported 60 GHz antenna.

Ref.	ε_r	-10dB S_{11} BW(%) (GHz-GHz)	3 dB-Gain BW(%) (GHz-GHz)	Peak Gain (dBi)	Size(mm^3) (λ_0^3)
[9]	2.2	15% (57.2-67.3)	20.4% (57-69)	8.6	11 × 11 × 0.033 (2.2×2.2×0.066)
[25]	5.9	14.5% (57-66)	14.5% (57-66)	6.3	6 × 6 ×1.5 (1.2×1.2×0.3)
[26]	3.02	9.1% (59.3-65)	9.1% (59.3-65)	10.02	12.8 × 10.87 × 0.597 (2.56×2.17 ×0.78)
[27]	n.a.	15% (55-64)	14.5% (57-66)	6	11 × 11 × 1 (2.2×2.2×0.2)
[28]	2.2	16.6%* (55-65)	n.a.	4	11.9 × 14.7 × 0.25 (2.38×2.94 ×0.05)
[29]	2.2	1.86% (59.4-60.6)	n.a.	9.29	12 × 16.4 × 0.127 (2.4×3.28× 0.0254)
[30]	6	23% (53-67)	18.3% (56-67)	6.9	2.44×2.44× 0.138 (0.49×0.49 ×0.028)
This work	3.27	44.7%* (44.2-69.7) 17.8% (57.6-68.8) 26.8%** (50.4-66.5)	25.8% (54-70)	11.42	6.4 × 6.4 × 0.375 (1.28×1.28 ×0.075)

* -8dB S_{11} BW
** Simulated

ground or probe is sensed by the reference horn antenna, so it is difficult to accurately measure the radiation pattern. Therefore, in the case of the E-plane, the radiation pattern was measured in the region of $-30° \leq \theta \leq 60°$. The S-parameter and radiation pattern measurements are conducted using a GSG probe. Fig. 14 shows the simulated and measured S_{11} values for the proposed antenna array. The simulated S_{11} is 16.1GHz(26.8%) ranging from 50.4 to 66.5GHz. The measured results are in good agreement with the simulated result although −10-dB S_{11} bandwidth decreases because the pole at 52.5 GHz is down-shifted to 50 GHz. This is presumably because the fabrication dimensions of the L-probe are differ from simulation values. Nevertheless, the measured −8-dB and −10-dB S_{11} bandwidth shows 25.5 GHz(=44.7%) ranging from 44.2 to 69.7 GHz, and 11.2GHz(=17.8%) ranging from 57.6 to 68.8 GHz, respectively.

Although the S_{11} value is below −8 dB, which exceeds −10 dB, the mismatched loss of S_{11} for −10 dB is 0.5 dB and the mismatched loss of S_{11} for −8 dB is 0.73 dB, and the deterioration of the realized gain is only 0.23 dB.

Fig. 15 shows the simulated and measured realized gains and realized efficiency for the proposed antenna array. The peak gain is 11.42 dBi and the 3-dB gain bandwidth ranges from 54 to 70 GHz (=25.8% fractional bandwidth). The measured realized efficiency is ranging from 73% to 96% in 60GHz unlicensed band(57-66GHz). Fig. 16 shows the simulated and measured E-plane and H-plane radiation patterns for frequencies of 57, 62, and 66 GHz for the proposed antenna array. The measured results agree with the simulated results for co-polarization. For cross-polarization, the measured cross-polarization level is higher than the simulated value because the reference horn antenna senses the co-polarized radiated field reflected from the probe or other measurement systems. Moreover, the discrepancy between the simulated and measured radiation patterns and boresight gain can correspond to the result of the horn antenna, which senses the radiated field reflected from the probe or other measurement systems. This in turn results in a distorted measured gain in the E-plane.

Table 1 shows a comparison of the reported 60-GHz antennas. S_{11} was distorted to −8dB due to errors in fabrication, but the insertion loss corresponding to −8dB S_{11} was 0.73 dB, so it was judged that there was no problem in actual use, and −8dB S_{11} was also added to the comparison table. The proposed antenna exhibits the widest bandwidth performance when compared with that of the compact antenna reported in the literature.

IV. CONCLUSION

In this study, a 60-GHz wideband L-probe circular slotted E-shaped patch antenna array is presented. The contributions of the study can be summarized as follows: 1) An E-shaped patch is added to the L-probe to further expand the bandwidth of the existing L-probe patch. 2) The E-shaped slot is modified to a circular slot to improve the overall performance, including the radiation pattern, S_{11}, and cross-polarization of the original E-shaped patch antenna element. The proposed antenna array reveals a peak gain of 11.42 dBi, 25.8% fractional 3-dB gain bandwidth, and 44.7% −8 dB S_{11} bandwidth with a size of 6.4 mm × 6.4 mm × 0.375 mm.

REFERENCES

[1] *FCC Rules for 60 GHz Operation: CFR 47 Part 15.255*, Federal Commun. Commission, Oct. 2010.
[2] K. Okada, N. Li, K. Matsushita, K. Bunsen, R. Murakami, A. Musa, T. Sato, H. Asada, N. Takayama, S. Ito, and W. Chaivipas, "A 60-GHz 16QAM/8PSK/QPSK/BPSK direct-conversion transceiver for IEEE 802.15.3c," *IEEE J. Solid-State Circuits*, vol. 46, no. 12, pp. 2988–3004, Dec. 2011.
[3] K. Okada, R. Minami, Y. Tsukui, S. Kawai, Y. Seo, S. Sato, S. Kondo, T. Ueno, Y. Takeuchi, T. Yamaguchi, and A. Musa, "A 64-QAM 60 GHz CMOS transceiver with 4-channel bonding," in *IEEE Int. Solid-State Circuits Conf. (ISSCC) Dig. Tech. Papers*, Feb. 2014, pp. 346–347.
[4] M. Boers, B. Afshar, I. Vassiliou, S. Sarkar, S. T. Nicolson, E. Adabi, B. G. Perumana, T. Chalvatzis, S. Kavvadias, P. Sen, and W. L. Chan, "A 16TX/16RX 60 GHz 802.11ad chipset with single coaxial interface and polarization diversity," in *IEEE Int. Solid-State Circuits Conf. (ISSCC) Dig. Tech. Papers*, Feb. 2014, pp. 344–345.
[5] R. Chair, C.-L. Mak, K.-F. Lee, K.-M. Luk, and A. A. Kishk, "Miniature wide-band half U-slot and half E-shaped patch antennas," *IEEE Trans. Antennas Propag.*, vol. 53, no. 8, pp. 2645–2652, Aug. 2005.
[6] R. Wu, S. Kawai, Y. Seo, N. Fajri, K. Kimura, S. Sato, S. Kondo, T. Ueno, T. Siriburanon, S. Maki, and B. Liu, "A 42Gb/s 60 GHz CMOS transceiver for IEEE 802.11ay," in *IEEE Int. Solid-State Circuits Conf. (ISSCC) Dig. Tech. Papers*, Feb. 2016, pp. 248–249.

[7] H. Sun, Y.-X. Guo, and Z. Wang, "60-GHz circularly polarized U-slot patch antenna array on LTCC," *IEEE Trans. Antennas Propag.*, vol. 61, no. 1, pp. 430–435, Jan. 2013.
[8] K.-F. Lee, S. L. S. Yang, and A. A. Kishk, "Dual- and multiband U-slot patch antennas," *IEEE Antennas Wireless Propag. Lett.*, vol. 7, pp. 645–647, 2008.
[9] T. H. Jang, H. Y. Kim, D. M. Kang, S. H. Kim, and C. S. Park, "60 GHz low-profile, wideband dual-polarized U-slot coupled patch antenna with high isolation," *IEEE Trans. Antennas Propag.*, vol. 67, no. 7, pp. 4453–4462, Jul. 2019.
[10] S.-L. S. Yang, A. A. Kishk, and F.-L. Kai, "Frequency reconfigurable U-slot microstrip patch antenna," *IEEE Antennas Wireless Propag. Lett.*, vol. 7, pp. 127–129, 2008.
[11] F. Yang, X.-X. Zhang, X. Ye, and Y. R. Samii, "Wide-band E-shaped patch antennas for wireless communications," *IEEE Trans. Antennas Propag.*, vol. 49, no. 7, pp. 1094–1100, Jul. 2001.
[12] W. Yang and J. Zhou, "Wideband low-profile substrate integrated waveguide cavity-backed E-shaped patch antenna," *IEEE Antennas Wireless Propag. Lett.*, vol. 12, pp. 143–146, 2013.
[13] Y. Ge, K. P. Esselle, and T. S. Bird, "E-shaped patch antennas for high-speed wireless networks," *IEEE Trans. Antennas Propag.*, vol. 52, no. 12, pp. 3213–3219, Dec. 2004.
[14] K. Noguchi, H. Rajagopalan, and Y. Rahmat-Samii, "Design of wideband/dual-band E-shaped patch antennas with the transmission line mode theory," *IEEE Trans. Antennas Propag.*, vol. 64, no. 4, pp. 1183–1192, Apr. 2016.
[15] J. Yin, Q. Wu, C. Yu, H. Wang, and W. Hong, "Broadband symmetrical E-shaped patch antenna with multimode resonance for 5G millimeter-wave applications," *IEEE Trans. Antennas Propag.*, vol. 67, no. 7, pp. 4474–4483, Jul. 2019.
[16] K. M. Luk, Y. X. Guo, K. F. Lee, and Y. L. Chow, "L-probe proximity fed U-slot patch antenna," *Electron. Lett.*, vol. 34, no. 19, pp. 1806–1807, Sep. 1998.
[17] L. Wang, Y. X. Guo, and W. X. Sheng, "Wideband high-gain 60-GHz LTCC L-probe patch antenna array with a soft surface," *IEEE Trans. Antennas Propag.*, vol. 61, no. 4, pp. 1802–1809, Apr. 2013.
[18] K. L. Lau and K. M. Luk, "A wideband dual-polarized L-probe stacked patch antenna array," *IEEE Antennas Wireless Propag. Lett.*, vol. 6, pp. 529–532, 2007.
[19] Y.-X. Guo, C.-L. Mak, K.-M. Luk, and K.-F. Lee, "Analysis and design of L-probe proximity fed-patch antennas," *IEEE Trans. Antennas Propag.*, vol. 49, no. 2, pp. 145–149, Feb. 2001.
[20] J. Park, H.-G. Na, and S.-H. Baik, "Design of a modified L-probe fed microstrip patch antenna," *IEEE Antennas Wireless Propag. Lett.*, vol. 3, pp. 117–119, 2004.
[21] S.-H. Wi, Y.-S. Lee, and J.-G. Yook, "Wideband microstrip patch antenna with U-shaped parasitic elements," *IEEE Trans. Antennas Propag.*, vol. 55, no. 4, pp. 1196–1199, Apr. 2007.
[22] T. H. Jang, H. Y. Kim, H. H. Bae, and C. S. Park, "Wideband E-shaped patch antenna with parasitic strip for 60-GHz unlicensed band application," in *Proc. Int. Symp. Antennas Propag. (ISAP)*, 2018, pp. 1–2.
[23] K. D. Xu, H. Xu, Y. Liu, J. Li, and Q. H. Liu, "Microstrip patch antennas with multiple parasitic patches and shorting vias for bandwidth enhancement," *IEEE Access*, vol. 6, pp. 11624–11633, 2018.
[24] J.-F. Lin and Q.-X. Chu, "Enhancing bandwidth of CP microstrip antenna by using parasitic patches in annular sector shapes to control electric field components," *IEEE Antennas Wireless Propag. Lett.*, vol. 17, no. 5, pp. 924–927, May 2018.
[25] H. Y. Kim, T. H. Jang, H. H. Bae, and C. S. Park, "A 60 GHz compact multidirectional-beam antenna-in-package for mobile devices," *IEEE Antennas Wireless Propag. Lett.*, vol. 18, no. 11, pp. 2434–2438, Nov. 2019.
[26] S. R. Govindarajulu, R. Hokayem, and E. A. Alwan, "A 60 GHz millimeter-wave antenna array for 3D antenna-in-package applications," *IEEE Access*, vol. 9, pp. 143307–143314, 2021.
[27] D. Titz, R. Pilard, F. Gianesello, F. Ferrero, C. Luxey, P. Brachat, G. Jacquemod, and D. Gloria, "Industrial HTCC antenna-module SiP for 60-GHz applications," *IEEE Antennas Wireless Propag. Lett.*, vol. 11, pp. 576–579, 2012.
[28] K. Trzebiatowski, M. Rzymowski, L. Kulas, and K. Nyka, "Simple 60 GHz switched beam antenna for 5G millimeter-wave applications," *IEEE Antennas Wireless Propag. Lett.*, vol. 20, no. 1, pp. 38–42, Jan. 2021.
[29] Y. Hong and J. Choi, "60 GHz patch antenna array with parasitic elements for smart glasses," *IEEE Antennas Wireless Propag. Lett.*, vol. 17, no. 7, pp. 1252–1256, Jul. 2018.
[30] A. Rashidian, S. Jafarlou, A. Tomkins, K. Law, M. Tazlauanu, and K. Hayashi, "Compact 60 GHz phased-array antennas with enhanced radiation properties in flip-chip BGA packages," *IEEE Trans. Antennas Propag.*, vol. 67, no. 3, pp. 1605–1619, Mar. 2019.

TAEHWAN JANG (Member, IEEE) received the B.S. degree from the Department of Electronic Engineering, Hanyang University, Ansan, South Korea, in 2014, and the Ph.D. degree in electronic engineering from the Korea Advanced Institute of Science and Technology (KAIST), Daejeon, South Korea, in 2019. Since 2022, he has been with the Samsung Advanced Institute of Technology (SAIT), Suwon, South Korea, as a Staff Researcher. Since 2022, he has been with Hanyang University, where he is currently an Assistant Professor. His research interests include millimeter-wave antenna, and CMOS RF circuits and systems.

CHUL SOON PARK received the B.S. degree from Seoul National University, Seoul, South Korea, in 1980, and the M.S. and Ph.D. degrees in materials science and engineering from the Korea Advanced Institute of Science and Technology (KAIST), Daejeon, South Korea, in 1982 and 1985, respectively. From 1985 to 1999, he worked with the Electronics and Telecommunication Research Institute (ETRI), where he contributed to the development of semiconductor devices and circuits. From 1987 to 1989, he studied the very initial growth of group IV semiconductors during a visit to the AT&T Bell Laboratories, Murray Hill, NJ, USA. Since 1999, he has been with the Information and Communications University (which merged with KAIST, in 2009), Daejeon, where he is currently a Full Professor with the Engineering School and the Director of the Intelligent Radio Engineering Center. His research interests include reconfigurable RF integrated circuits (RFICs), millimeter-wave integrated circuits (ICs), and their system-on-chip (SoC)/system-on-package (SoP) integration.